Measurement 136 (2019) 185–200

Contents lists available at ScienceDirect

Measurement

journal homepage: www.elsevier.com/locate/measurement

An investigated reactive power measurements-based fault-identification scheme for teed transmission lines

Mohamed I. Zaki [a], Ragab A. El-Sehiemy [b,*], Ghada M. Amer [a], Fathy M. Abo El Enin [c]

[a] Electrical Engineering Department, Faculty of Engineering, Benha University, Egypt
[b] Electrical Engineering Department, Faculty of Engineering, Kafrelsheikh University, Kafrelsheikh, Egypt
[c] Electrical Engineering Department, Alexandria University, Alexandria, Egypt

ARTICLE INFO

Article history:
Received 28 August 2018
Received in revised form 10 December 2018
Accepted 21 December 2018
Available online 22 December 2018

Keywords:
Fault detection
Fault classification
Faulted phase identification
Teed circuits
Transmission lines
Reactive-power
Discrete wavelet transform

ABSTRACT

The process of fault-identification in teed transmission lines (TTLs) has considerable attention in recent years. In this line, this paper proposes a novel scheme for fault detection, classification and faulted-phase/s identification on the basis of reactive-power components of TTLs. The current and voltage measurements are collected from a single-end measuring system of teed circuits. Based on the filtering of measured currents and voltages signals using improved recursive wavelet transform, the reactive-power measurements are computed. Thereafter, the Wavelet Multi-Resolution Analysis Technique (WMRAT) is employed for decomposition of reactive-power measurements. An improved recursive wavelet (IRW) transform that has good time-frequency characteristics is proceed to remove dc offsets and harmonics from the measured signals. The ATP/EMTP package and MATLAB program are used to simulate the faulted cases and verify of operating the proposed fault-identification scheme. Simulation outcomes show that the proposed scheme has the capability to detect and classify different fault types in TTLs. The presented scheme is designated to be insensitive to different fault resistances, different fault locations, and inception angles. In addition, the proposed scheme is also tested under different technical aspects such as different sampling rates, different locations of the single-end measuring system, loading change and source parameters variation. The superiority of reactive-power compared with active power measurements during faults occurrence is also investigated to show the notability of the proposed scheme. The obtained results corroborate that the proposed scheme can be correctly identified different fault types and locations along the line.

1. Introduction

In teed transmission lines (TTLs) protection, it is required to classify faults and identify faulty phase/s. These functions are necessary to decline the time abruption and speed up electrical service restoration. Furthermore, they are used to corroborate the single-pole tripping techniques and auto-reclosing mechanisms [1]. The process of fault-identification through TTLs has more complexity due to serious conditions which are listed as follows [2]:

- The effect of in-feed at the third terminal.
- The influence of out-feed at teed point.
- Asymmetrical lengths of teed branches.
- Different source impedance at each terminal.

All these severe conditions may cause fault-identification complexities. However, the fast and accurate fault-identification technique is required to alleviate the impact of faults on the reliability of teed circuits [3].

The fault-identification on one and two terminals transmission lines has obtained worthy interest through previous studies [4–11]. The current and/or voltage measurements were utilized in various algorithms to detect and classify faults on electrical networks. These measurements were customized from single or double end measuring systems. While the two terminal lines are not efficacy for EHV network in comparison with teed circuits [12]. Thus, multi-terminal circuits are attracting widespread interests due to economic merits. Therefore, the different approaches have been presented in some research papers [2,12–26] to protect TTLs. Depending on obtainability of measurements, fault-identification methods can be classified into two; using synchronized measurements from all ends [2,12–18,24,25] or double ends [19]. In [2,12–14], the authors introduced algorithms that were designed to identify the faults based on synchronized voltages and currents

* Corresponding author.
E-mail address: elsehiemy@eng.kfs.edu.eg (R.A. El-Sehiemy).

https://doi.org/10.1016/j.measurement.2018.12.068
0263-2241/

from all ends of TTLs. Also, the use of current measurements from all three-line terminals and locally voltage measurements at relay installed are considered in [15]. In contrast, the fault-identification methods in [16,24,25], were based on synchronized currents data from all ends. Refs. [17,18] employed synchronized voltage measurements to pinpoint the fault-identification where the effect of current-transformer saturation was eliminated to avoid the impact of the current transformer error. With advent of the synchronization measurements, a new method in [19] is proposed using the currents and voltages from two terminals of teed circuits.

On the other side, authors in [20–22] presented fault identification schemes based on unsynchronized data measurements, which were collected from all ends of three terminal circuits. In [20], the fault detection algorithm was developed by using the unsynchronized currents and voltages from all ends, based on the synchronization angle deviation between fault and healthy conditions. The fault-identification algorithm in [21] was developed by using an analytical method based on negative-sequence voltages at fault point corresponding to negative-sequence voltages in three terminals. An integrated wavelet-support vector machine method based travelling wave for fault identification in teed circuits is proposed in [22], using unsynchronized data measurements from only two terminals.

In [23], the authors proposed protection scheme for teed circuit based on the apparent impedance from measurement data at only one terminal. The fault classification and faulted phase/s selection have several critical aspects in fault-identification studies on TTLs. Therefore, the fault classification scheme in [24] with the adaptive threshold for TTLs was proposed. Using DWT, the high-frequency components were extracted by using db6 that was used as mother wavelet. The main downside of this study has neglected the impact of fault resistance. In [25], the power spectrum density (PSD) and multiresolution analysis technique were utilized to determine the faulty phase/s. Ref. [26] addressed the fault classification scheme for teed circuits but it failed to identify the faulty phase/s.

Refs. [27–34] provided the recent publication in studying the impact of reactive power during and after faults for disturbance-identification. In [27], a review on the generalized instantaneous reactive-power computations was addressed. Based on wavelet coefficient of currents and voltages, the reactive-power was computed for studying the impact of it during and after fault occurrence [28]. In [29], the effect of reactive power was developed to discriminate between faults and power swing operating conditions. In [30], a comparative study around shunt and series reactive power compensation was presented using unified power flow controller (UPFC). The direction concept was developed in [31–33] to utilize the sourced voltage converter SVC and static synchronous compensator STATCOM for reactive power control during disturbance. To enhance the power transfer limit, the SVC and STATCOM were used to provide the reactive-power compensation during and after faults. Also, it reduced the variation of bus voltage, hence, improving the power system performance. In [34], the TCSC is allocated in transmission system in an optimal manner using differential evolution method for enhancing the operation of power systems and improve the management of reactive power. In [35], a method was presented to discrimination between permanent and transient faults by using DWT for shunt compensation transmission systems.

In the literature, most approaches have only concentrated on the fault detection and location techniques using with little attention to fault classification on TTLs. Also, some approaches for the fault-identification have been based on measurements data from two and three terminals of TTLs. Therefore, the current paper gives considerable considerations for these challenges. In the proposed scheme, a novel fault-identification scheme is presented based on the reactive-power influence during a fault occurrence. The measuring system is installed at one terminal of teed circuits to measure the voltages and currents data. Then, they are utilized to calculate the reactive-power signals, which are decomposed by using (WMRAT). Thereafter, the detail coefficients are derived from Daubechies (db1) that is used as mother wavelet. The salient features of this paper are summarized as follows:

- Developing the fault-identification scheme for TTLs.
- By using WMRAT, the impact of mother wavelet selection on the behaviour of the fault identification scheme.
- Studying the influence of different shunt-fault types, locations, fault resistances, inception angles, and sampling frequency variations.
- Testing the fault-identification scheme under different operating conditions such as different locations of the single-end measuring system, loading changes, and source parameters variations.
- A close accord assessment study between the proposed scheme and previous existing schemes in the literature is proceed to show the reliability of the proposed scheme.

This rest part of this paper is divided into five sections as: Section 2 introduces the wavelet transform technique. A new proposed methodology is presented in Section 3. Section 4 describes the studied system model and simulation cases for testing the TTLs model based on the proposed scheme. Thereafter, Section 5 discusses and evaluates the proposed fault-identification scheme for TTLs system. Finally, conclusions are drawn in Section 6.

2. Discrete wavelet transform based multi-resolution technique

Discrete Wavelet Transform (DWT) is considered the precise tool that is used to analyze the transient signal in the power system. Where any measured transient signals from the power system can be represented in time and frequency domain. The wavelet transform has been dependent on the multiresolution analysis technique that is developed to analyze the electrical signals as an alternative to DFT. For high-frequency signals, the high time resolution and low-frequency resolution are considered, while, for low-frequency signals, the low time resolution and high-frequency resolution are considered [36].

The DWT decomposes an original non-stationary signal into low and high frequencies components namely approximate and detail coefficients, respectively. These coefficients are considered as indices, which can be employed as distinctive characteristics for fault-identification methodology. As well, the choice of the basis function namely mother wavelet is a very crucial role in fault-identification techniques as mentioned in [36]. The wavelet coefficients can be mathematically expressed as [37] in (1) and (2). These equations can give approximation (A1) and detail (D1) coefficients at one level.

$$A1[k] = \sum_{n=-\infty}^{\infty} X[n] * L[n-2k] \quad (1)$$

$$D1[k] = \sum_{n=-\infty}^{\infty} X[n] * h[n-2k] \quad (2)$$

where X is the sampled signal, k represents the translation interval, L (n) and h(n) are scaling and wavelet filters.

In this study, the Daubechies (db1) wavelet is applied to decompose the reactive-power signals into detail coefficients, which can be employed to identify the faults on teed circuits. The fault-identification criteria in this approach are based on the maximum absolute value for these coefficients at one level of decomposition.

This paper applied the fault-identification strategy for deriving fault detection, classification, and faulted phase selection based on locally instantaneous signals. Based on single-end measuring system and reactive-power computation, the distinguished features of the proposed scheme compared with the existing schemes are:

(1) Selection of the impact of reactive-power corresponding to three phases as distinctive features-based DWT technique on TTLs.
(2) The proposed scheme can cope with high fault resistances compared to the most existing approaches such as current-based methods. This yields the compensation effect and makes the proposed method as suitable protection system for dealing with extreme severe scenarios.
(3) The novelty of the wavelet approach is based on the hybridization of the details' coefficients and their deviations according to three phases to identify different fault types in TTLs. In this direction, the DWT based details coefficients can be calculated soon after each sampling process, which is good aspect for practical real time applications.
(4) Local measured currents and voltages from one terminal of TTLs, are sufficient to make a correct decision based proposed scheme.
(5) The proposed scheme has been based on logical flow without using any classifier technique, hence, it is able to identify faults in TTLs in one stage, and it means that the proposed approach has high fast response against faults.

3. Proposed fault-identification scheme

This paper introduces a proposed scheme for fault detection, classification and faulted-phase/s identification on TTLs. The logical concept of the proposed scheme is entirely deterministic. It is based on the reactive-power impact during different fault cases. The usage of reactive-power measurements precisely depends on the reactance a long line, in TTLs the effect of all resistances is diminished in comparison to reactances [39,40]. When a fault occurred, a severe maximum current appears in TTLs. Thereby, the massive reactive power will find in TTLs. Since the fault currents and voltages will have several harmonics and decaying dc components, the computation of reactive power will be subject to errors and thus the accuracy will extremely deteriorate. Therefore, the voltage and current measurements involving sub-harmonics and decaying dc offset components must be filtrated. The authors in [44] proposes a filter design using improved recursive wavelet (IRW) transform that has good time–frequency characteristics to eliminate the DC offset and sub-harmonics. This filter has superior rejection capability of the exponentially decaying dc offsets and sub-harmonics. In this study, the IRW filter is proceed to eliminate the sub-harmonics and decaying dc components of the measured reactive power signals. Then, the computation of instantaneous reactive power based proposed identification scheme can be employed as follows:

$$\Delta V_{ab} = V_a - V_b \tag{3}$$

$$\Delta V_{bc} = V_b - V_c \tag{4}$$

$$\Delta V_{ca} = V_c - V_a \tag{5}$$

$$Q_a = I_a \times \Delta V_{bc} \tag{6}$$

$$Q_b = I_b \times \Delta V_{ca} \tag{7}$$

$$Q_c = I_c \times \Delta V_{ab} \tag{8}$$

where ΔV_{ab}, ΔV_{bc}, ΔV_{ca} are, respectively, called difference voltages between phases a-b, b-c, c-a. Also, V_a, V_b, V_c are, respectively, called voltages corresponding to three phases measured at relay point. Similarly, I_a, I_b, I_c are, respectively, called currents corresponding to three phases measured at the relay point. Finally, Q_a, Q_b, Q_c are denoted to reactive-power corresponding to three phases.

Thereafter, WMRAT is applied to extract the faulted features based on the reactive-power behaviour during fault conditions. The proposed scheme depends on db1 (mother-wavelet) which can be utilized to decompose the measured reactive-powers per phase. Using one stage of decomposition, the high-frequency components can be extracted. Then, their maximum absolute values can be computed and used as input to the proposed scheme.

In details, the proposed scheme is based on two hypotheses as:

- The first one is dependent on the maximum absolute value for the detail coefficients of reactive-power measurements.
- The second hypothesis is dependent on the deviation of the maximum absolute value of details between phases A, B, and C. As well, they can be used as indices in order to identify the different shunt-fault types on TTLs.

In this study, the fault classification and faulted-phase/s identification can be verified by using the adaptive threshold value, which is settled according to loading change on teed circuits that is estimated as (9). The complete flow diagram in Fig. 1 shows the procedure of fault-identification methodology that can be performed as follows:

- The sampled voltage and current measurements are gathered from the one-end measuring system on teed circuits.
- Filtering the measured sampled voltages and currents using IRW transform.
- Calculating the reactive-power measurements per phases (Q_a, Q_b, Q_c) according to Eqs. (6)–(8).
- Decomposing the reactive-powers measurement by using WMRAT and selecting db1 as mother wavelet at one level of decomposition. Also, the zero-sequence current is decomposed by using db1.
- Extracting the detail coefficients for reactive-power measurements and the approximate coefficients for zero-sequence current.
- Computing the maximum absolute value for zero-sequence current approximate coefficients (Ag) and reactive-power detail coefficients per phase which are denoted by (QD_a, QD_b, QD_c).
- After calculating (QD_a, QD_b, QD_c) the adaptive threshold value is estimated according to the load variation and/or different sampling frequencies used by using the following proposed Equ. (9) as:

$$D_{th} = \alpha * (QD_a + QD_b + QD_c)/(3 * \omega) \tag{9}$$

where: α is a correction factor and equal 1.045.
ω: An index of sampling rate value and can be chosen 0.5 for 3.2 kHz, 1 for 6.4 kHz, and 2 for 12.6 kHz.
- Finding the deviation of (QD_a, QD_b, QD_c) between each phase and others ($|\Delta Dab|$, $|\Delta Dbc|$, $|\Delta Dca|$).
- Applying the presented methodology for fault-identification as shown in Fig. 1 to detect and classify the faults and recognize the faulty phase/s.

In brief, the distinctive rules for identifying the faulty phases are summarized in Table 1 to facilitate and illustrate the proposed scheme.

3.1. Fault detection based on the self-adaptive threshold formula

Basically, the self-adaptive threshold formula (D_{th}) has been proposed to set the boundary between fault and healthy condi-

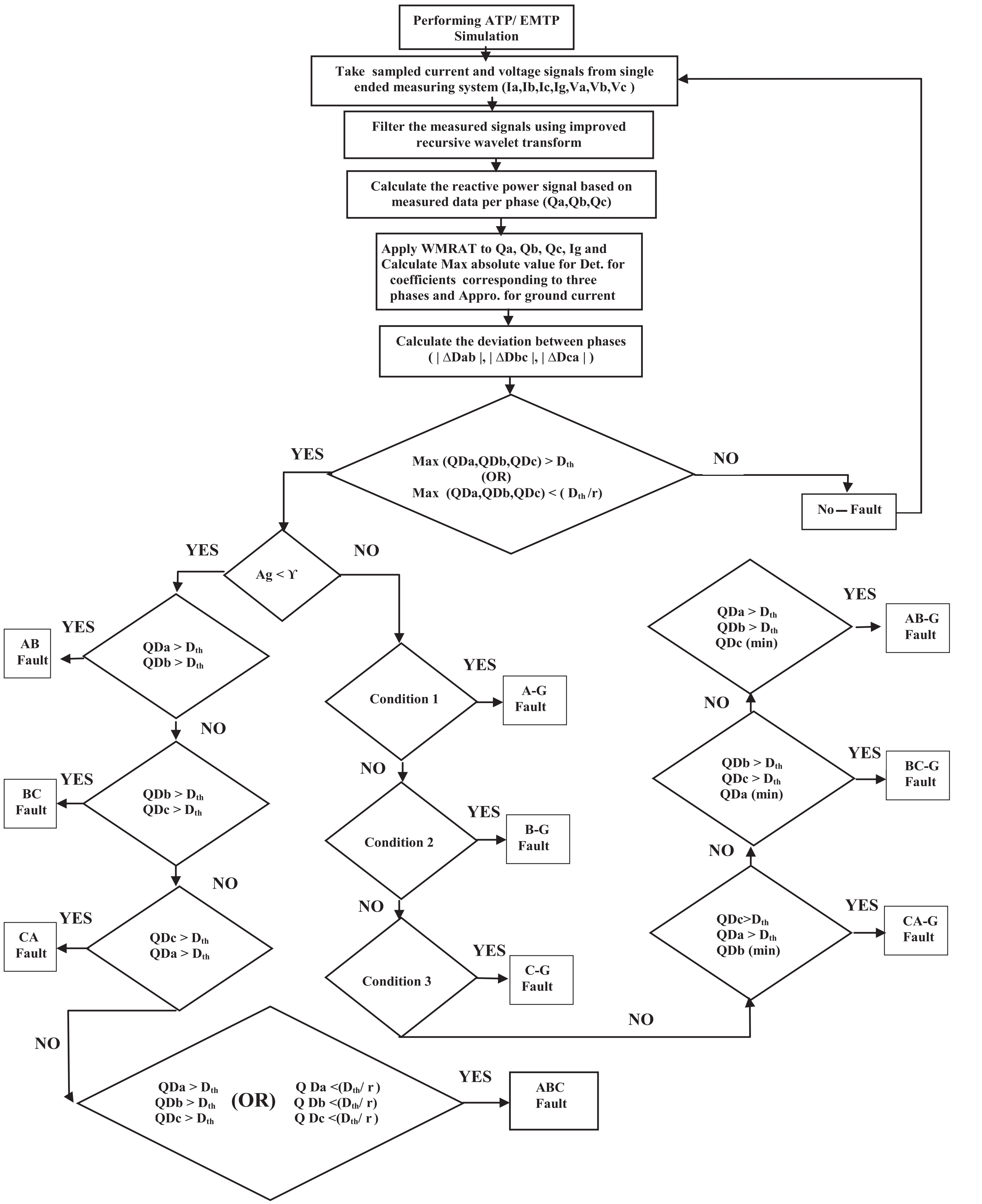

Fig. 1. Flow diagram for presented protection scheme.

tions. Whenever the value of QD_a, QD_b, QD_c exceeds the self-adaptive threshold value or declines to less than (D_{th}/r), a fault is detected. Where, r to represent the ratio of zero-sequence reactance to its positive-sequence reactance. It's noted that the choice of the self-adaptive threshold formula is a critical aspect for fault-identification on TTLs. Therefore, different test cases for the health situation with varying source impedances and power transfer angle values have been generated on TTLs as shown in Fig. 2. At

Table 1
Features rule for fault classification based on the reactive-power behavior.

Fault types	Criteria of the classification rules (QDa, QDb, QDc , |ΔDab|, |ΔDbc|, |ΔDca|)			Ag
AG	Condition (1)	QDa (max)	First criterion |ΔDab| (max), QDb < (D_{th} * β_2), QDc < (D_{th} * β_3) (OR) Second criterion |ΔDca| (max), QDb < (D_{th} * β_4), QDa < (D_{th} * β_5)	Ag > Υ
BG	Condition (2)	QDb (max)	First criterion |ΔDbc| (max), QDa < (D_{th} * β_2), QDc < (D_{th} * β_3) (OR) Second criterion |ΔDab| (max), QDc < (D_{th} * β_4), QDb < (D_{th} * β_5)	Ag > Υ
CG	Condition (2)	QDc (max)	First criterion |ΔDca| (max), QDa < (D_{th} * β_2), QDb < (D_{th} * β_3) (OR) Second criterion |ΔDbc| (max), QDa < (D_{th} * β_4), QDc < (D_{th} * β_5)	Ag > Υ
ABG		QDa > D_{th}	QDb > D_{th}	Ag > Υ
BCG		QDb > D_{th}	QDc > D_{th}	Ag> Υ
CAG		QDc > D_{th}	QDa > D_{th}	Ag > Υ
AB		QDa > D_{th}	QDb > D_{th}	Ag < Υ
BC		QDb > D_{th}	QDc > D_{th}	Ag < Υ
CA		QDc > D_{th}	QDa > D_{th}	Ag < Υ
ABC	Group (1)		QDa > D_{th}, QDb > D_{th}, QDc > D_{th}	Ag < Υ
	Group (2)		QDa < (D_{th}/r), QDb < (D_{th}/r), QDc < (D_{th}/r)	

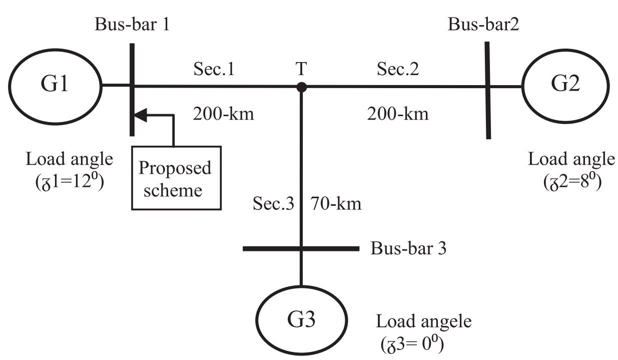

Fig. 2. Tested Single line diagram for TTLs model.

simultaneously, huge numbers of fault cases with varying fault parameters (fault type, fault resistance, fault inception angle, fault location) have been analyzed with/without different operating conditions.

3.2. Fault classification based on the self-adaptive threshold formula

For single line fault (SL-G), the deviation of details between phases should be taken into account in order to recognize the faulty phase/s. For example, if a fault happens in phase A, the condition (1) is applied which includes two criteria. Where each criterion comprises some rules as shown in Table1, can be defined as a first criterion. Also, the second criterion includes some rules are considered as referred to in the same Table 1. The proposed criteria for each condition are presented to overcome some severe conditions in TTLs during shunt-faults. For example, if AG fault occurrence, the details of reactive-power in phase A are the highest value compared to sound phases in both criteria. If the first or second criterion is investigated in condition (1) will indicate to single line fault (SL-G) in phase A. As similarly for condition (2) or condition (3), if any one of them is investigated will refer to SL-G fault occurrence in phase B or phase C, respectively.

For double line to ground fault (DL-G) and line to line fault (L-L), the fault-identification scheme is based on the maximum absolute value of reactive-power details in faulty phase/s. As expected, the details of healthy phases are the lowest value compared to the faulty phases. In addition, the detail coefficients of faulted phases exceed the self-adaptive threshold. Also, the approximate coefficient for zero-sequence current (Ag) is used to distinguish between DL-G fault and L-L fault as follows:

- If Ag > Υ the fault involves the ground.
- If Ag < Υ the fault is between phases without any ground, where Υ is a very small value close to zero.

For three-phase fault (L-L-L), the fault-identification scheme can be classified into two groups; the first group involves some rules which depend on the fact that the maximum absolute values, QD_a, QD_b, and QD_c, are greater than D_{th} and Ag close to zero. The second group also involves some rules which depend on the fact that the maximum absolute values, QD_a, QD_b, and QD_c, are lower than (D_{th}/r) and Ag near to zero. The second group represents the worst case that can investigate when a solid three-phase fault occurs at close to the relay point. In either case, if any rules in the group (1) or group (2) are investigated, this means that the three-phase fault has happened.

4. Application

4.1. Description of TTLs model

A tested system model 500-kV, 50-Hz, TTLs system is depicted as Fig. 2. Each end of the TTLs model is fed through sources namely G_1, G_2, and G_3, respectively. The simulated test system has three transmission lines, which are connected as teed configuration. These transmission lines are denoted by Sec 1, Sec 2, Sec 3 and their lengths are 200 km, 200 km, and 70 km, respectively. The transmission lines and source parameters are shown as [38] and are specified in Appendix A.

4.2. Simulating of tested TTLs model based the proposed scheme

The single line diagram of tested TTLs in Fig. 2 is simulated using ATP/EMTP package. Also, several fault parameters are considered to generate the simulation fault data. The measuring system is adjusted at the single-end on TTLs to measure the current and voltage quantities. Then, both sampled voltage and current signals are loaded into the algorithm in the MATLAB software. The voltages and currents are filtrated then used to compute the sampled reactive-power per phase during the fault occurrence. A sampling frequency of 6.4 kHz (128 samples per cycle) is used for analysis.

The reactive-power measurements at faulty cases are analyzed and decomposed using db1 that is represented as mother wavelet. The proposed scheme needs to the high-frequency components which are extracted from the wavelet technique. Also, it needs to extract the low-frequency component of zero-sequence current. The distinctive features extractions are fed into the proposed scheme and around 846 test cases are simulated. The different operating conditions in the teed transmission lines have been considered. Also, all fault parameters are considered as different fault resistances, inception angles, and fault locations. Several studied cases are executed using testing TTLs which are depicted in the following section.

4.3. Test cases

The proposed scheme is evaluated for different fault situations to prove its effectiveness. In addition, the considerable tests carried out to give more reliable operation for the presented scheme. Furthermore, these tests show that the proposed scheme has the capability to detect and classify faults in teed circuits under variation of fault parameters. Seven simulated fault cases are applied in the TTLs model as depicted in Fig. 2. The simulation results of fault cases have been recorded in Table 3–4, respectively under various simulated shunt-fault types and different fault parameters. The description of these test cases is presented as follows:

Case 1: All shunt-fault types are simulated under different fault parameters (fault instant: 0.05 s, transition resistance: 0.0001 Ω, and fault location: at bus-bar 1). The results of the fault-identification scheme are reported in Table 3;
Case 2: Various shunt-fault types are applied considering different fault parameters (fault instant: 0.06 s, transition resistance: 100 Ω, and fault location: at the teed point). The fault-identification scheme results also are reported in Table 3;
Case 3: Various shunt-fault types are applied considering different fault parameters (fault instant: 0.07 s, transition resistance: 110 Ω, and fault location: at bus-bar 3). The results of the fault-identification scheme are reported in Table 4;
Case 4: Various shunt-fault types are tested under different fault parameters (fault instant: 0.065 s, transition resistance: 600 Ω, and fault location: at bus-bar 2). The results of the fault-identification algorithm are reported in Table 4;
Case 5: The shunt-fault occurrence with different fault parameters (fault instant: 0.08 s, transition resistance: 10 Ω, and fault location: 100 km away from bus-bar 1) are considered;
Case 6: The shunt-fault occurrence with different fault parameters such as (fault instant: 0.08 s, transition resistance: 40 Ω, and fault location: 100 km away from bus-bar 2) are considered; and
Case 7: The shunt-fault occurrence with different fault parameters (fault instant: 0.09 s, transition resistance: 3 Ω, and fault location: at the teed point) are considered.

4.4. The selection of suitable mother-wavelet based fault-identification scheme

Among various types of mother-wavelets, the optimal selection of suitable mother-wavelet is a critical task. The choice of mother-wavelet also depends on a nature of the application. In addition, the optimum wavelet details' level, which includes the hidden fault features, is chosen corresponding to its energy contents. For this purpose, the proposed indices (QD_a, QD_b, QD_c) in this study are highly based on the type of mother wavelet. As consequence, the results may be drastically changed corresponding to the selected mother-wavelet type [41]. Table 2 shows the impact of different mother-wavelets as Daubechies (db), Biorthogonal (bior), Symmlet (sym), Coiflet (coif) at different healthy and faulty cases. It can be observed that the mother-wavelet db1 has high performance and fast response compared to other mother wavelets used. Therefore, this study can select (db1) as a suitable mother-wavelet used.

5. Results and performance-evaluation

To evaluate the proposed fault-identification method, the depicted TTLs in Section 4 is simulated and different fault cases are carried out. Then, the measured signals are collected from measuring instruments that are located at bus-bar 1 as shown in Fig. 2. Thus, the reactive-power signals can be measured and also the detail coefficients can be obtained by using db1 that is used as

Table 2
The impact of mother wavelets selection based the proposed fault-identification scheme.

Mother wavelet	Fault Case #	Fault type	QDa	QDb	QDc	Dth	Ag	Total-elapsed time (s)	Fault-identification scheme
db1	Sound case		$1.4289 * 10^7$	$1.4336 * 10^7$	$1.4342 * 10^7$	$1.4965 * 10^7$	$\sim = 0$	2.088223	No-Fault
db1	Case1	B-G	$1.013 * 10^7$	$24.53 * 10^7$	$2.139 * 10^7$		$1.529 * 10^4$		√
db1	Case2	AB-G	$3.364 * 10^7$	$3.730 * 10^7$	$1.416 * 10^7$		$1.310 * 10^3$		√
db1	Case3	AB	$3.785 * 10^7$	$2.906 * 10^7$	$1.252 * 10^7$		$\sim = 0$		√
db6		Sound	101.3788	109.5333	106.4017	110.5308	$\sim = 0$	3.302129	No- Fault
db6	Case4	A-G	112.3882	104.8429	102.7704		38.275		X
db6	Case5	AB-G	875.1638	745.7027	65.8356		$5.87 * 10^3$		√
db6	Case1	ABC	0.0044	0.0055	0.0058		$\sim = 0$		√
biro2.2		Sound	$7.0357 * 10^5$	$7.0150 * 10^5$	$7.0399 * 10^5$	$7.3465 * 10^5$	$\sim = 0$	3.503264	No- Fault
biro2.2	Case4	B-G	$7.2725 * 10^5$	$7.5597 * 10^5$	$6.9647 * 10^5$		38.376		√
biro2.2	Case1	AB-G	$6.5210 * 10^6$	$6.3797 * 10^6$	4.7720		$1.605 * 10^4$		√
sym3		Sound	$1.0902 * 10^5$	$1.0865 * 10^5$	$1.0906 * 10^5$	$1.1381 * 10^5$	$\sim = 0$	3.050842	No- Fault
sym3	Case7	CA	$6.8721 * 10^5$	$5.234 * 10^5$	$6.1323 * 10^5$		$\sim = 0$		√
sym3	Case4	B-G	$1.1270 * 10^5$	$1.1705 * 10^5$	$1.0812 * 10^5$		38.311		√
coif1		Sound	$1.1579 * 10^6$	$1.1532 * 10^6$	$1.1578 * 10^6$	$1.2083 * 10^6$	$\sim = 0$	3.013148	No- Fault
coif1	Case4	B-G	$1.1968 * 10^6$	$1.2437 * 10^6$	$1.1460 * 10^6$		38.293		√
coif1	Case1	A-G	$1.9795 * 10^7$	$1.7269 * 10^6$	$8.2060 * 10^5$		$1.604 * 10^4$		√

√ ———————— Correct decision, X———————— False decision.

Table 3
The simulation results for fault cases 1, 2.

Fault type	Fault instant(s)	QDa * **10^7**	QDb * **10^7**	QDc * **10^7**	**|ΔDab|** * **10^7**	**|ΔDbc|** * **10^7**	**|ΔDca|** * **10^7**	Ag * **10^3**	Identifying Faulty Phase
Sound case	1.428	1.433	1.434					0	Healthy
Case 1, R_F = 0.0001 Ω									
AG	0.05	24.57	2.136	1.015	22.442	1.1213	23.563	15.29	AG
BG	0.05	1.013	24.53	2.139	23.525	22.399	1.1258	15.28	BG
CG	0.05	2.133	1.016	24.51	1.1167	23.501	22.384	15.22	CG
ABG	0.05	13.33	12.96	0	0.3785	12.960	13.338	16.99	ABG
BCG	0.05	0	13.30	12.99	13.306	0.3131	12.993	17.00	BCG
ACG	0.05	12.97	0	13.31	12.973	13.316	0.3427	2.720	ACG
AB	0.05	16.92	15.74	0				0	AB
BC	0.05	0	16.96	15.75				0	BC
CA	0.05	15.71	0	16.93				0	AC
ABC	0.05	0	0	0				0	ABC
Case 2, R_F = 100 Ω									
AG	0.06	3.554	1.367	1.485	2.1868	0.1117	2.0690	0.585	AG
BG	0.06	1.480	3.546	1.368	2.0664	2.1778	0.1113	1.335	BG
CG	0.06	1.365	1.484	3.557	0.1194	2.0730	2.1925	1.336	CG
ABG	0.06	3.364	3.730	1.416	0.3659	2.3137	1.9477	1.310	ABG
BCG	0.06	1.411	3.359	3.716	1.9474	0.3678	2.3052	1.301	BCG
ACG	0.06	3.730	1.414	3.354	2.3163	1.9400	3.7623	0.968	ACG
AB	0.06	4.964	4.394	1.185				0	AB
BC	0.06	1.184	4.952	4.400				0	BC
CA	0.06	4.387	1.182	4.956				0	AC
ABC	0.06	3.514	3.522	3.515				0	ABC

Table 4
The simulation results for cases 3, 4.

Faulttype	Fault instant (s)	QDa * **10^7**	QDb * **10^7**	QDc * **10^7**	**|ΔDab|** * **10^7**	**|ΔDbc|** * **10^7**	**|ΔDca|** * **10^7**	Ag * **10^3**	Identifying Faulty Phases
Sound case	1.428	1.433	1.434		0	Healthy			
Case 3, R_F = 110 Ω									
AG	0.05	2.471	1.323	1.709	1.1478	0.3856	0.7622	0.485	AG
BG	0.05	1.704	2.480	1.323	0.7755	1.1567	0.3811	0.486	BG
CG	0.05	1.326	1.706	2.478	0.3804	0.7714	1.1520	0.258	CG
ABG	0.05	2.648	2.550	1.576	0.0996	0.9741	1.0738	0.480	ABG
BCG	0.05	1.575	2.639	2.548	1.0641	0.0911	0.9730	0.480	BCG
ACG	0.05	2.541	1.579	2.651	0.9623	1.0708	0.1084	0.292	ACG
AB	0.05	3.785	2.906	1.252				0	
BC	0.05	1.256	3.77	2.900				0	
CA	0.05	2.900	1.254	3.778				0	
ABC	0.05	2.672	2.66	2.671				0	
Case 4, R_F = 600 Ω									
AG	0.06	1.540	1.419	1.480	0.1201	0.6074	0.0059	0.019	AG
BG	0.06	1.476	1.537	1.416	0.6117	0.1208	0.5972	0.038	BG
CG	0.06	1.417	1.479	1.535	0.0627	0.0526	0.1179	0.038	CG
ABG	0.06	1.584	1.521	1.462	0.0632	0.0583	0.1216	0.037	ABG
BCG	0.06	1.461	1.583	1.527	0.1209	0.5508	0.0628	0.038	BCG
ACG	0.06	1.528	1.465	1.578	0.0628	0.1128	0.0499	0.026	ACG
AB	0.06	1.777	1.516	1.415				0	
BC	0.06	1.411	1.774	1.510				0	
CA	0.06	1.516	1.416	1.772				0	
ABC	0.06	1.572	1.566	1.571				0	

mother-wavelet. Thereafter, the maximum absolute value of details (QD_a, QD_b, QD_c) and their deviation (|**ΔDab**|, |**ΔDbc**|, |**ΔDca**|) are computed. These indices are used as input for the proposed fault-identification scheme as shown in Fig. 1. The fault-identification results have been compared to the simulated fault type and faulty phase to make sure the validation of the proposed method. The total execution time of fault-identification needs 2.5 ms.

Four correction factors β_1, β_2, β_3, β_4, are chosen according to several studies have been carried out in Appendix B. We found that these correction factors are as 3.2772, 1.3073, 1.5856, 1.4078, and 2.0604, respectively.

Accordingly, the flexibility of the proposed fault-identification scheme evaluation is assessed according the following categories:

(1) fault specification;

In this category, six cases are considered as:

(a) Effect of variation in shunt-fault type.
(b) Effect of variation in transition resistances (fault resistances).
(c) Effect of variation in fault locations.
(d) Effect of variation in fault inception instants.

(e) Effect of a closed-up solid fault at relay point.
(f) Effect of sampling rate variation.

(2) system parameters variation;

In this category, three cases are considered as:

a) Influence of source impedance variations.
b) Effect of change loading in teed circuits.
c) Effect of varying location of the single-end measuring system.

Added to that, the assessment study is employed between the proposed scheme and existing schemes in the literature.

5.1. The flexibility of the proposed scheme against varied fault specification

5.1.1. Effect of variation in shunt-fault types

All shunt-fault types have been tested on the proposed fault-identification scheme at different fault cases to evaluate it. The corresponding results are given by the proposed fault-identification scheme of fault cases 1–4 can be summarized in Tables 3 and 4, respectively. In Table 3, it is noted from case 1 results that the maximum absolute values of reactive-power details coefficient during ABC fault equal zero. Especially, once the three-phase closed-up solid fault occurs, which refers to the fault happens near to the relay point, the reactance of the system is near to zero. Thereby, the details of reactive-powers per phases are diminished. As a result, the close-up three phase solid faults cannot be detected. To solve this problem, the proposed technique is designed to identify these faults, whenever, the value of QD_a, QD_b, QD_c exceed the self-adaptive threshold (D_{th}) value or decline to less than (D_{th}/r). From all results that are shown in Tables 3 and 4, it is cleared that the proposed scheme can be able to cover all shunt-fault types at different fault conditions.

5.1.2. Effect of variation in transition resistances (fault resistances)

Indeed, the impact of increasing fault-resistance value may be caused considerable damping in the magnitude of the current signal. To prove the efficacy of the proposed fault-identification scheme against this issue, seven fault cases with different values

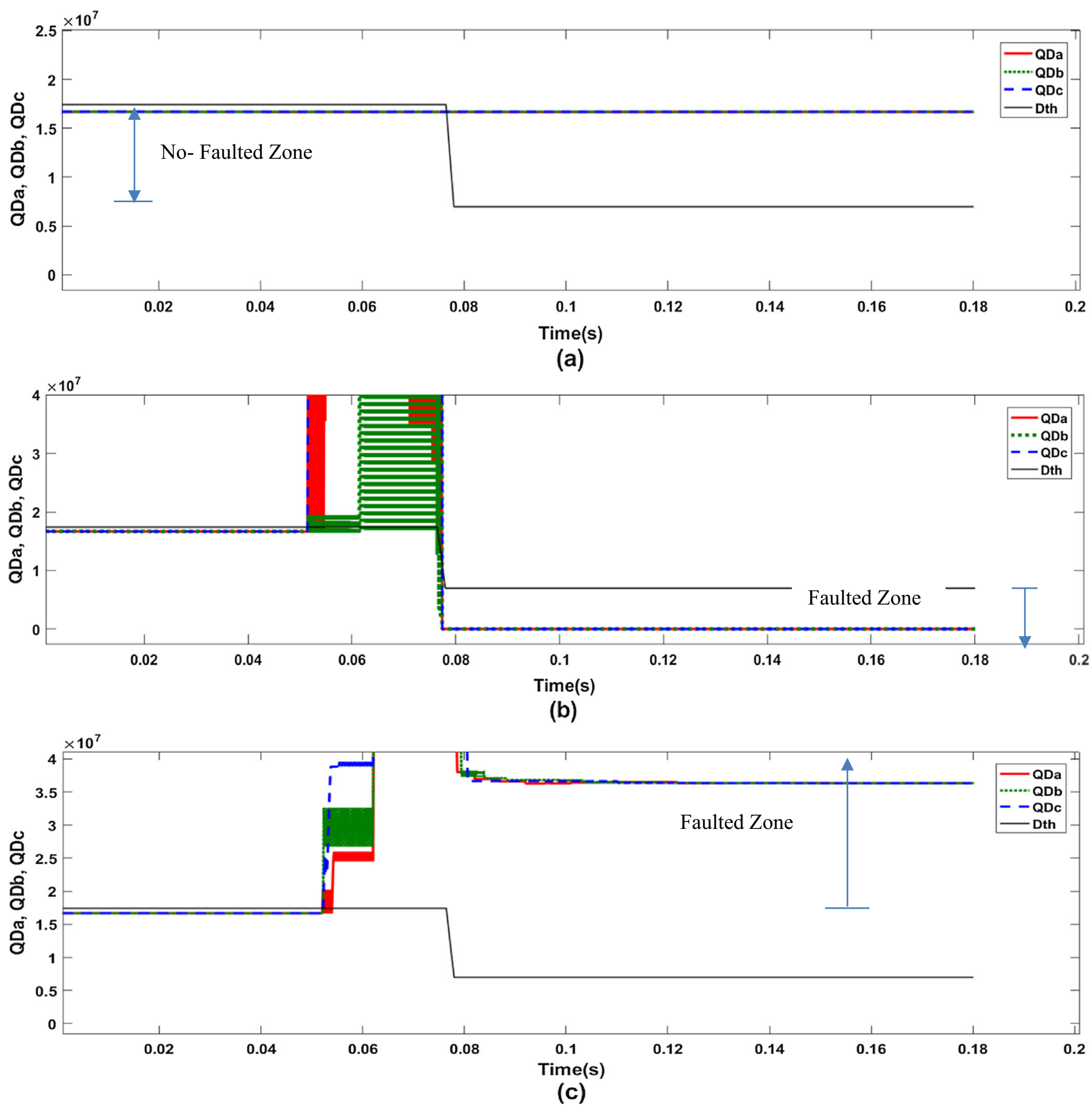

Fig. 3. The variation in adaptive threshold values (D_{th} and D_{th}/r both) and value of QD_a, QD_b, QD_c at different fault locations. (a) At heath case; (b) three-phase closed-up solid fault at bus 1; (c) three-phase fault case 1 at the teed point.

of fault-resistances are simulated. Tables 3 and 4 illustrate that the proposed scheme is immune to the effect of fault resistances in a wide range from (R_F = 0–600 Ω). Therefore, the proposed scheme can be still insensitive to high fault-resistance and can give a right response.

5.1.3. Effect of variation in fault locations

The performance of the proposed fault-identification scheme has been verified by simulating faults at different locations on the TTLs model. In all fault cases 1–7, different fault locations at bus-bar 1, 2, 3, teed point, and 100 km away from bus-bar 1, 2 are tested with varying all fault types, different fault resistances, and inception angles. The obtained results have been reported in Table 3 and 4 at different positions in order to prove an efficacy of the proposed scheme. Fig. 3 shows the variation in adaptive threshold values (D_{th} and D_{th}/r both) and value of QD_a, QD_b, QD_c at different fault locations. Fig. 3(a) illustrates the variation value of QD_a, QD_b, QD_c at healthy condition (without fault in system). It is noted from Fig. 3(a) that these values are bounded between adaptive thresholds (D_{th} and D_{th}/r). On the contrary, when a fault occurred, the value of QD_a, QD_b, QD_c exceed the self-adaptive threshold (D_{th}) value or decline to less than (D_{th}/r) as shown in Fig. 3(b) and (c). It is cleared that the proposed scheme can be able to cover all shunt-fault types at different fault locations.

5.1.4. Effect of fault inception instants variation

To evaluate the Fault Inception Angles (FIAs) influence on the proposed fault-identification scheme behave, a scenario in fault case 1 is simulated. It is well known that the fault inception angle of single line faults are high drastic when close to FIA is 90° [42]. Therefore, the selected fault inception angles were 0, 90, 180, and 360 from phase (A) voltage zero-crossing (four cases), the proposed scheme is verified under different FIAs and the obtained results are shown in Fig. 4. Fig. 4(d) shows the variation value of QD_a with four values of fault inception angles in A-G fault during fault case 1. For all fault inception angles analyzed, the proposed scheme properly classified and identified the faulty phase.

5.1.5. Effect of a closed-up fault during solid faults at the relay point

The challenge of mutual coupling between phases is found in case of SL-G faults during solid faults at relay point. For this reason, both maximum absolute value of phases A and B are higher than the adaptive threshold value as depicted in Fig. 5. Thence, it is referring to double line to ground fault which was considered in phase A and B in most previous studies. To overcome this challenge, the proposed scheme based on both maximum absolute values of QD_a, QD_b, QD_c and their deviations. Another challenge is found in case of three-phase solid fault at relay point. We find that the maximum absolute values of reactive-powers details per phases are diminished as shown in Fig. 3(b). To solve this problem, the proposed scheme is designed to identify these faults, whenever, the value of QD_a, QD_b, QD_c exceed the self-adaptive threshold (D_{th}) value or decline to less than (D_{th}/r). Consequently, the proposed scheme has the capability of identifying these fault types.

5.1.6. Effect of sampling rate variation

Sampling frequencies utilized during the analog to digital conversion (ADC) of current and voltage signals have a big impact on transient based fault-identification schemes [43]. To evaluate the proposed fault-identification scheme, the variations of sampling frequencies (3.2 kHz, 6.4 kHz, and 12.6 kHz) are studied. Different simulated fault types are carried out at R_F is 80 Ω (random value) and faults are initiated at 0.07 s. The obtained results are depicted in Fig. 6(a), (b), and (c). For all sampling frequencies used, the proposed scheme properly classified and identified the faulty phase. Therefore, the proposed scheme is valid for all sampling frequencies. Because the adaptive threshold value is settled according to the index value of sampling rate (ω), see to (9).

5.2. The flexibility of proposed scheme against varied system parameters

The fault-identification scheme should remain immune to any healthy change or disturbance in the system. Accordingly, we should also authenticate the performance of proposed scheme for healthy disturbance i.e. the case of a change in load angle (sudden

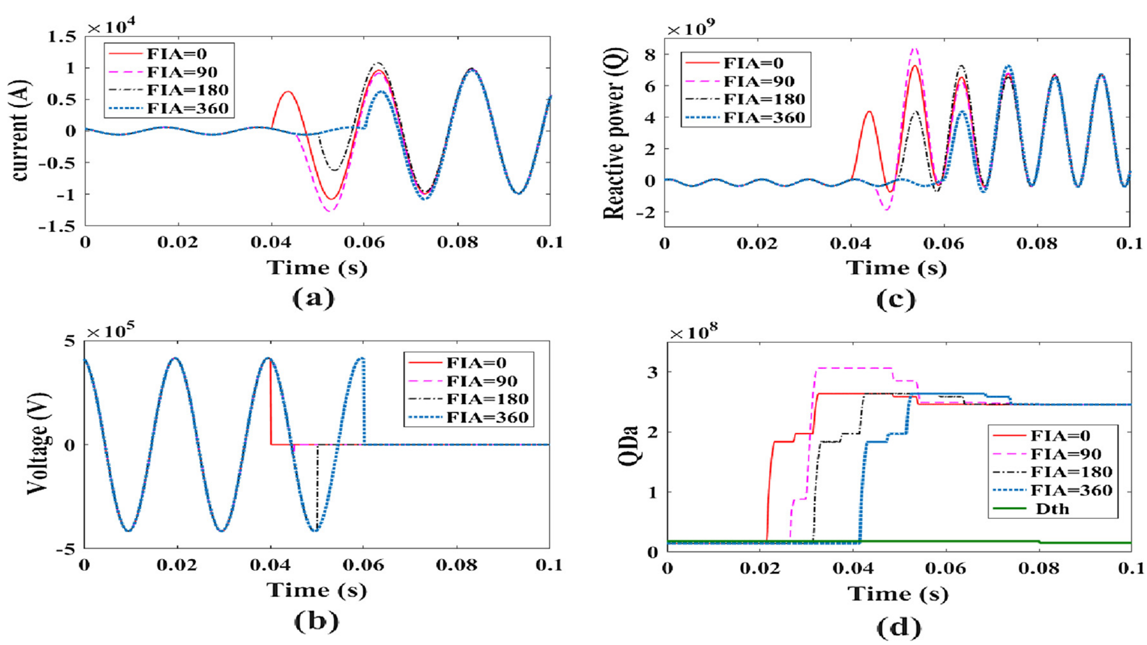

Fig. 4. The performance of the proposed fault-identification technique with various fault inception angles (0, 90, 180, and 360) for case 1. (a) The fault current waveforms in phase A; (b) The fault voltage waveforms in phase A, (c) The fault reactive power waveform in phase A; and (d) Details coefficient of reactive power for phase A.

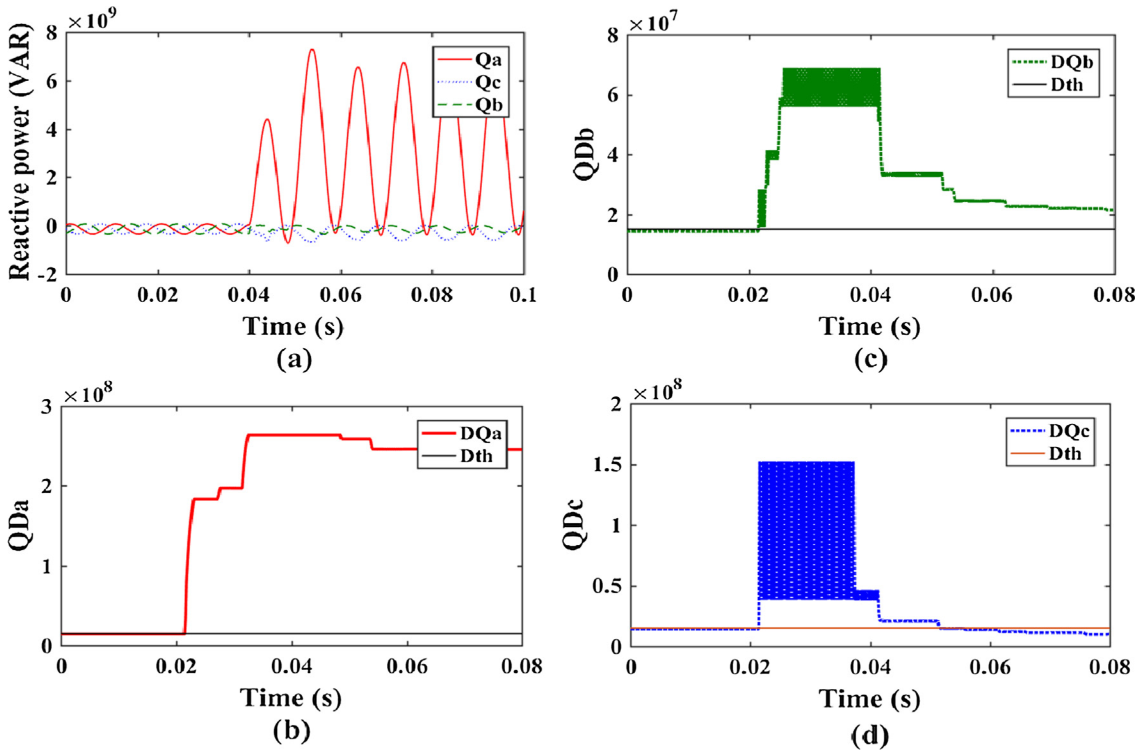

Fig. 5. The behaviour of the maximum absolute value of reactive power details coefficients in presence of solidly single line to ground fault i.e. $R_F = 0\,\Omega$: (a) three phases reactive power waveforms; (b) Details coefficient of reactive power for phase A; (c) Details coefficient of reactive power for phase B; Details coefficient of reactive power for phase C.

change), and source impedance. The self-adaptive threshold reacts at the instant of healthy change happened and it settles a new value according to the impact of healthy disturbance. Furthermore, the change is not noticeable in the adaptive threshold value under healthy disturbance. It is observed from Fig. 7 that the proposed scheme is insusceptible to the impact of healthy disturbance because it depends on the adaptive threshold. In addition, it is also able to detect, classify and identify the faulty phase.

5.2.1. Influence of source impedance variations

The impact of the source impedance variations on the proposed fault-identification scheme is considered for all fault types. The reliability of the classification scheme with a variety of source impedance (Z_3) was verified by perturbing (Z_3) by ±15% of base value. The tests as shown in Table 5 also prove that the source impedance variation cannot affect the fault-identification scheme. Due to two reasons, firstly, the values of details (QD_a, QD_b, QD_c) do not remarkably change. Secondly, the threshold values are adapted and computed according to newly defined source impedance.

5.2.2. Effect of change loading in teed circuits

The reliability of the proposed fault-identification scheme against loads variation is investigated by connecting different loads at buses G_1, G_2, and G_3 at different load angles. To validate the performance of the proposed scheme, cases 6–7 with various fault types and different load angles are simulated. Table 6 shows the obtained results of the impact of load variations based on varying the loading angle (δ) at G_2. Accordingly, the self-adaptive threshold reacts at the instant of load variation and it settles to a new value according to new loading settled. It can be seen that even with sufficient variation in load; the proposed fault-identification scheme can still detect and classify faults.

5.2.3. Effect of varying location of the single-end measuring system

The proposed fault-identification scheme is also tested at a different location of single-end measuring system at bus-bar 1 or bus-bar 2 or bus-bar 3. Table 7 shows the effect of the measuring system at various locations in the presence of the faulted situation in case 5. It is cleared that the proposed scheme possesses the high availability for detecting and classifying faults at different single-end measuring system locations.

5.3. Verification of the superiority of selecting reactive-power measurements against active power measurements

A comparison between active- and reactive-power measurements are required to show the superiority of the scheme. Table 8 shows the behavior of both active- and reactive-power details coefficients during SL-G fault in phase A. Several simulations are investigated that cover wide range of fault resistances at different fault locations to evaluate the superiority of the reactive power based proposed method. In low fault resistance closed to relay point, the performance of the proposed method based active-power failed to identify correctly the SL-G fault as shown in Table 8. The reactive power measurements reveal their distinct data and their capability of identifying the faulty phase correctly. In addition, as exposed in Table 8, the use of reactive power measurements for fault type classification and faulted phase identification makes the approach robust to different fault situations. The performance of proposed method for fault-identification is tested for a range of R_f from 0.001 to 600 Ω. The results show that the performance of the proposed method based reactive power has the superiority against using active power. Therefore, in this paper, we depend on the reactive power measurements for proposed method to identify different fault types.

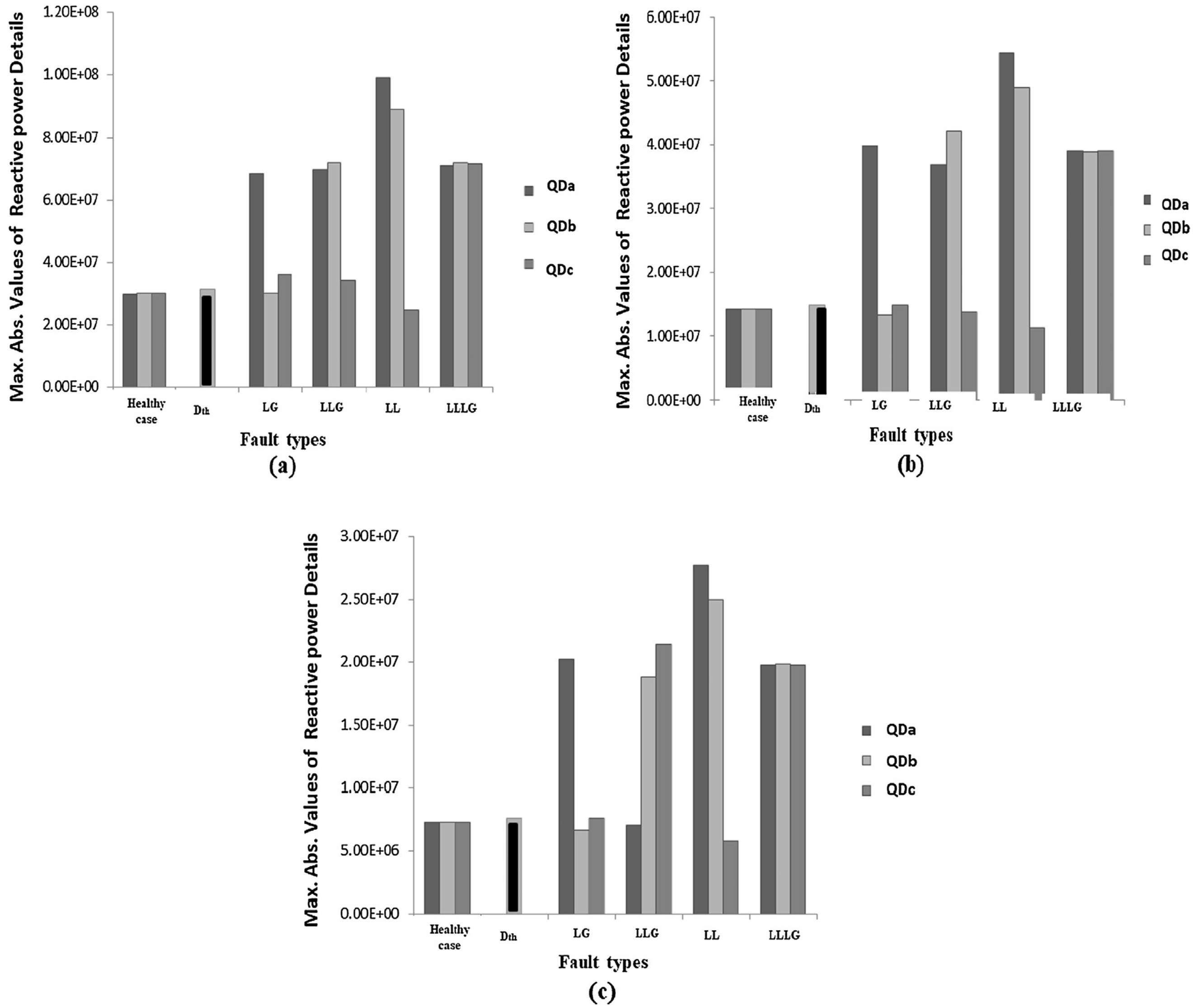

Fig. 6. The behavior of the maximum absolute value of reactive power details coefficients at different sampling frequencies: (a) at 3.2 kHz; (b) at 6.4 kHz; (c) at 12.6 kHz.

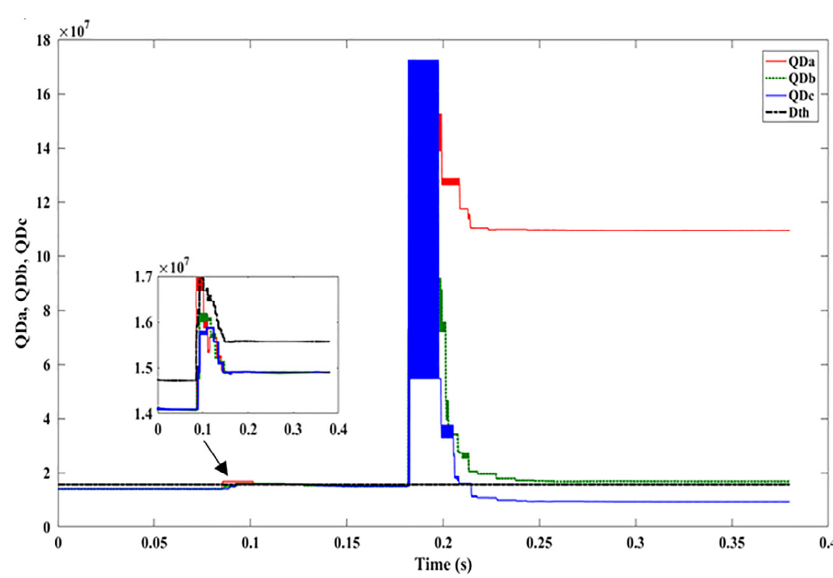

Fig. 7. The impact of healthy disturbance with/without fault occurrence.

Table 5
The effect of loading change based on changes in the load angle through G2.

Source impedance (Z_3) (Ω)	Fault type	Fault case	QDa * 10^6	QDb * 10^6	QDc * 10^6	Ag * 10^3	Fault classification
Base value, Z_3	Sound		14.28	14.33	14.34	0	Healthy
Z_{30} = 17 + 42.390i	D_{th} = 14.96579 * 10^6						
Z_{31} = 14 + 28.25i	AG	Case 7	76.6969	7.9049	15.188	4.1354	AG_ Fault
	ABG	Case7	77.330	73.581	7.2188	3.4853	ABG_ Fault
Varied by + 15% of base value, Z_3	Sound		14.472	14.505	14.518	0	Healthy
Z_{30} = 19.55 + 48.748i	D_{th} = 15.15075 * 10^6						
Z_{31} = 16.1 + 32.487i	AG	Case7	77.222	7.3737	15.253	4.1019	AG_ Fault
	ABG	Case7	77.398	73.980	7.0574	3.4525	ABG_ Fault
Varied by 15 –% of base value, Z_3	Sound		14.909	14.923	14.874	0	Healthy
Z_{30} = 14.45 + 36.031i	D_{th} = 16.258458 * 10^6						
Z_{31} = 11.9 + 24.0125i	AG	Case7	76.627	8.6633	14.976	4.1195	AG_ Fault
	ABG	Case7	77.255	73.690	7.4232	3.536	ABG_ Fault

Z_{30} and Z_{31} denote to zero and positive sequence components of the source impedance at G_3, respectively.

Table 6
The effect of loading change based on changing in the load angle through G2.

Loading angle (δ)	Fault type	Faulty case	Load current value(A)RMS	Details coefficients Characteristics				Ag * 10^3	Reactive-power measurements based classification scheme decision
				QDa * **10^7**	QDb * **10^7**	QDc * **10^7**	Dth * **10^7**		
8°	Healthy	––––––	405.559	1.4289	1.4342	1.4315	1.496589	=~0	No fault
	AG	Case 6		3.4619	1.0781	1.6478		1.0711	AG
	BCG	Case 7		0.7468	7.6582	7.2354		3.4948	BCG
6°	Healthy	–––––	432.187	1.5241	1.5266	1.5228	1.593102	=~0	No fault
	ABG	Case 6		3.6900	3.9222	1.3429		1.2030	ABG
	CG	Case 7		0.8283	1.6397	7.6508		3.3775	CG
4°	Healthy	–––––	458.892	1.6182	1.6165	1.6131	1.68865	=~0	No fault
	BC	Case 6		1.2352	5.0547	3.6788		=~0	BC
	ABC	Case 7		5.3227	5.3504	5.3491		=~0	ABC
−6°	Healthy	–––––	592.420	2.0676	2.0666	2.0598	2.15757	=~0	No fault
	CAG	Case 6		4.1982	1.7936	4.1082		0.2469	CAG
	BG	Case 7		2.1164	7.6344	1.2801		4.0492	BG
−4°	Healthy	––––	565.819	1.9765	1.9799	1.9751	2.06565	=~0	No fault
	ABC	Case 6		3.9905	3.9916	3.9760		=~0	ABC
	CA	Case 7		6.5424	1.0712	9.2191			CA
−12°	Healthy	––––	671.571	2.3205	2.3223	2.3263	2.4275	=~0	No fault
	ABG	Case 6		4.2824	4.3378	2.0115		1.1929	ABG
	CG	Case 7		1.4954	2.3529	7.6409		3.1010	CG

Table 7
The behavior of the proposed scheme against different single measuring system locations.

Single measuring location	Fault type	Fault case	QDa * 10^6	QDb * 10^6	QDc * 10^6	Fault classification
Bus- bar 1	Sound		14.28	14.33	14.34	Healthy
	D_{th} = 1.496579 * 10^7					
	AG	Case 5	110.00	15.17	9.80	AG_ Fault
	ABG	Case5	88.00	103.3	6.99	ABG_ Fault
Bus- bar 2	Sound		8.883	8.8645	8.8634	Healthy
	D_{th} = 9.2692893 * 10^6					
	AG	Case5	38.034	3.7008	10.227	AG_ Fault
	ABG	Case5	44.227	45.342	4.5941	ABG_ Fault
Bus- bar 3	Sound		15.580	15.515	15.580	Healthy
	D_{th} = 16.258458 * 10^6					
	AG	Case5	60.680	13.835	12.712	AG_ Fault
	ABG	Case5	53.159	65.614	9.6314	ABG_ Fault

5.4. Practical implementation based proposed scheme

In real application for online fault detection and classification, the measuring system is active all the time to collect the instantaneous signals and compute the reactive power measurements at relay point. For smart online monitoring, the intelligent electronics devices IEDs and self-powered non-intrusive sensors are developed as an alternatively to traditional measuring systems [45]. These advanced techniques in measurements can guarantee fast reaction to fault situations and the correct functioning of online measuring system-based sensing monitors' networks. Once a fault arrives to protective relay location, the fault-identification scheme requires only 16 samples, it is applied to obtain fault features over 1/8 of a cycle data window at sampling rate 6.4 kHz. The proposed identification scheme detects and classifies all fault types at 2.5 ms from the time which the fault begins. This is relatively high-

Table 8
A comparative study between active- and reactive-power measurements fault identification schemes.

Fault type	R_f (Ω)	Fault location (km)	Input data (Power type)	QDa * 10^7	QDb * 10^7	QDc * 10^7	PDa * 10^8	PDb * 10^8	PDc * 10^8	Ag * 10^3	Relay decision	Identifying Faulty Phase
Sound case			Reactive	1.428	1.433	1.434				0	Healthy	√
			Active				2.962	2.968	2.969			√
AG	0.001	Relay point	Reactive	24.52	2.132	1.021				16.234	AG	√
AG			Active				1.8335	7.1038	3.5138		BG	x
AG	1	Relay point	Reactive	24.338	2.0884	0.9602				15.275	AG	√
AG			Active				1.7992	7.0103	3.4232		BG	x
AG	3	50 km from G_1	Reactive	15.401	1.7548	0.9423				9.8693	AG	√
AG			Active				8.6118	5.2110	1.5898		ABG	x
AG	10	50 kmfrom G_1	Reactive	14.663	1.8467	0.7937				8.8112	AG	√
AG			Active				11.484	4.9395	1.3787		ABG	x
AG	20	50 kmfrom G_1	Reactive	13.385	1.9251	0.6690				7.1344	AG	√
AG			Active				14.738	4.5337	1.2851		ABG	x
AG	25	Relay point	Reactive	17.282	2.105	0.3856				9.2564	AG	√
AG			Active				21.848	4.8521	1.2080		ABG	x
AG	60	100 km from G_2	Reactive	7.2890	1.6065	0.9722				2.4895	AG	√
AG			Active				13.392	3.3410	2.2978		AG	√
AG	100	Teed point	Reactive	3.5501	1.3680	1.4795				0.6312	AG	√
AG			Active				7.7732	2.9423	3.2807		AG	√
AG	200	G_3	Reactive	2.0215	1.3837	1.5909				0.1682	AG	√
AG			Active				4.5018	2.9854	3.3549		AG	√
AG	400	100 km From G_2	Reactive	1.7805	1.4112	1.1410				0.0685	AG	√
AG			Active				3.8874	2.9654	3.0811		AG	√
AG	600	G_2	Reactive	1.5359	1.4147	1.4743				0.0216	AG	√
AG			Active				3.2639	2.9670	3.0654		AG	√

Table 9
Assessment study between the proposed fault-identification scheme with existing schemes in the literature.

Ref. #	System Config.	SuitableR_F (Ω) range	Input data	Sampling frequency	Technique Used	Fault detection	Fault classification	Faulted-Phase Identification
[1]	Two-terminal Lines	0–100	Voltages & currents form single end	200 kHz	DWT&ANN	√	√	X
[5]	Two-terminal Lines	1–300	Currents from single end	6.4 kHz	DWT&KBT	√	√	√
[6]	Two-terminal Lines	5–60	Voltages & currents	4 kHz	DWT&SVM	√	√	√
[7]	Two-terminal Lines	3–50	Currents from single end	0.6.4 kHz	DWT	√	√	√
[11]	Two-terminal Lines	10–100	Symmetrical components reactive power	———————	———————	√	√	√
[37]	Two-terminal Lines	——————	Currents from two ends	19.2 kHz	DWT	√	√	X
[42]	Two-terminal Lines	0–100	Voltages & currents	15.36 kHz	MODWT	√	X	X
[2]	Teed-transmission Lines	0–100	Voltage s& currents from all and/or single ends	240 kHz	DWT& TW	√	X	X
[12]	Teed-transmission Lines	0–50	Voltages & currentsform all ends	2.4 kHz	Dynamic parameter estimator	√	X	X
[16]	Teed-transmission lines	0–350	Currents form all ends	20 kHz	CWT	√	X	X
[17]	Teed-transmission lines	1–300	Voltages form all ends	600 kHz	HT&DWT	√ √	X	X
[24]	Teed-transmission lines	————	Currents form all ends	———————	DWT	√	X	X
[25]	Teed-transmission lines	—————	Currents form all ends	20 kHz	PSD&MRA	√	X	X
[26]	Teed-transmission lines	—————	Currents form local terminal	———————	MRA	√	√	X
Proposed scheme	Teed transmission lines	0–600	Reactive power per phase from single end	6.4 kHz	DWT	√	√	√

speed identification scheme which is validated for online fault-identification. Thereafter, the developed real time WMRA coefficients at one level is used to process the reactive power signals and extract the details corresponding three phases. The adaptive threshold value is adapted online with a new settled value according to the absolute maximum values of details for on period in moving window identification scheme at normal operation based on duration time concept. Based on the value of details and their deviations according to three phases we can detect and classify faults online. The proposed scheme does not need to training data and has low computational burden. Further, the fault-identification scheme-based DWT and reactive power measurements are online and can be implemented on the existing smart protective relaying infrastructure.

5.5. Comparative assessment

The comparison of the proposed fault-identification scheme with closed existing schemes in the literature is investigated to explain the superiority of the proposed technique. For comparison purpose, Table 9 is presented to illustrate the salient features of the proposed fault-identification scheme. The assessment study is carried out based on the type of system configuration, suitable R_F (Ω) range, input data, and the sampling frequency used. Refs. [1,2,17,25,37], and [42] require a very high sampling frequency which increases the computational burden. Whereas, the proposed scheme requires low sampling frequencies as 3.2 kHz, 6.4 kHz, 12.6 kHz which reduce the computational burden. The major shortages in [24–26,7,36] are noticed that they overlook the effect of fault resistances R_{Fs} in their studies. Whereas, the proposed scheme can detect, classify and identify faulted-Phase a wide range of fault resistance from 0 up-to 600 Ω compared to others schemes.

The salient features of the proposed fault-identification scheme compared to existing schemes can be depicted below:

- For fault-identification (detection, classification, and faulted-phase selection), the same feature extraction stage can be applied to enhance overall operation speed of the proposed scheme.
- The logical concept of the proposed scheme is entirely deterministic, that allows implementing the proposed scheme without needing any historical data acquisition.
- The proposed scheme is based on a single-end measuring system and no need for a communication system (fast and data transfer). So, the proposed scheme has less impact on the external conditions.
- In the proposed fault-identification scheme, no need for additional classifier techniques, moreover, it is regarded high speed because it depends upon the discriminative feature's extraction in one stage.
- The proposed scheme requires low sampling frequencies as 3.2 kHz, 6.4 kHz, and 12.6 kHz which reduce the computational burden.

6. Conclusions

This paper has presented a novel fault-identification scheme based on the influence of reactive-power behavior in the TTLs system. Using the single-end measuring system, the current and voltage signals have been measured and filtrated, and then reactive-power measurements have been computed. The proposed fault-identification scheme depends on the adaptive threshold value that has been estimated according to loads and system parameters variation in TTLs. To do so, the maximum absolute value of the reactive-power details obtained using the WMRAT are computed and analysed. The performance of the fault-identification scheme has been testing a 500-kV teed transmission lines using ATP/EMTP package. To illustrate the proposed scheme evaluation, the flexibility of the proposed scheme against fault and system parameters variations has been discussed and elaborated in details.

The corresponding salient merits of the proposed scheme can be concluded as follows:

- Developed the fault-identification scheme based on TTLs.
- The superiority of using the reactive-power as an alternating to active power measurements during faults occurrence has been achieved in this study.
- The logical principle has been entirely deterministic, that facilitates the realization of the proposed scheme.
- The proposed scheme used the improved recursive wavelet filter to eliminate the dc components and harmonics associated with fault signals, hence, the performance of proposed scheme is very high accurate.
- The proposed scheme does not need the time-synchronization of measuring devices.
- Studied the impact of mother wavelet selection based on (WMRAT) to select the optimal mother wavelet.
- Studied the influence of different shunt-faults, locations, fault resistances, inception angles, and sampling frequencies variations on TTLs.
- Tested the fault-identification scheme under different operating conditions such as different locations of the single-end measuring system, loading changes, and source impedance variations.

The suggested future works for testing the proposed fault-identification scheme involve but not limited to the following issues, as:

- Studying the impact of three-terminal transformers on TTLs model.
- Testing the behaviour of the proposed scheme for the TTLs model that constitutes double-circuits and compensated lines.
- Investigating discrimination criteria between internal and external faults (just outside the bus-bar 1, bus-bar 2, and bus-bar 3) on TTLs.
- Studying the impact of voltage sag during single line to ground fault on TTLs model.
- Solving problems associated with multi-lateral distribution systems.
- Developing the fault section identification in TTLs and fault location scheme.

Appendix A: System Data

- Transmission lines parameters
  R_1 = 0.018399 (Ω/km): Positive sequence resistance
  R_0 = 0.04612 (Ω/km): Zero sequence resistance
  $L_1 = 0.8858 * 10^{-3}$ (H/km): Positive sequence inductance
  $L_0 = 2.654 * 10^{-3}$ (H/km): Zero sequence inductance
  $C_1 = 13.06 * 10^{-9}$ (F/km): Positive sequence capacitance

- Source parameters

  G_1 : V_1 = 500 kV 12° (substation-1), 50 Hz
  G_2 : V_2 = 500 kV 8° (substation-2), 50 Hz
  G_3 : V_3 = 500 kV 0° (substation-3), 50 Hz

Appendix B. Correction factors computation

The selection value of ratio of zero- to positive-reactances (x_0/x_1) is dependent on the position and material that is used for ground system in overhead lines. The typically value for this ratio is located in range from 2 to 3.55 [40]. Because of the mutual reactance and adding 3 times ground reactance, the ratio x_0/x_1 may vary over according to different voltage levels and system configurations. Accordingly, the ground fault identification is highly dependent on x_0/x_1 ratio. In the proposed scheme for single line to ground fault identification, four correction factors are used to enhance the performance of proposed scheme to cover wide range of ground faults. The correction factors are computed as follows:

$$\text{At first Consider } r = \frac{X_0}{X_1} \tag{B.1}$$

Then use this ratio r to compute the suggested correction factors according to the correlated equations that are deduced for different real networks after several studies as follows:

The first correction factor is computed using the following equation:

$$\beta_1 = \frac{r+1}{r} \tag{B.2}$$

The second correction factor is computed through the following equation:

$$\beta_2 = \frac{r^2(1+\beta_1) + \beta_1(r\beta_1 - 1)}{r^2\beta_1^2} \tag{B.3}$$

Table B.1
Optimal settings for the proposed scheme for different systems.

Transmission lines data	[38]	[7]	[4]	[23]	[21]	[26]	[6]	Analysis	
Configuration	Teed Circuits	Two Terminal Circuits	One Terminal Circuit	Teed Circuits	Multi Terminal Circuits	Teed circuits	Two Terminal Circuits	Mean value	Average Deviation
Voltage level	500 kV	500 kV	220 kV	220 kV	735 kV	66 KV	400 KV		
r	2.99616	3.1521	3.4782	3.539	3.452	2.794	3.529	3.2772	0.254104
β_1	1.3337	1.3172	1.2875	1.2822	1.2896	1.3579	1.2833	1.3073	0.024792
β_2	1.56	1.5763	1.6034	1.6084	1.6013	1.5423	1.6080	1.5856	0.022404
β_3	1.445	1.4549	1.3701	1.3620	1.3735	1.4859	1.3635	1.4078	0.046363
β_4	2.0070	2.1006	2.0339	2.0224	2.0386	2.1954	2.0249	2.0604	0.050057

Table B.2
The simulation results for teed circuits 66 kV Delta realistic network.

Fault type	R_f Ω	Location Km	QDa * 10^5	QDb * 10^5	QDc * 10^5	|ΔDab| * 10^5	|ΔDbc| * 10^5	|ΔDca| * 10^5	Ag	Identifying Faulty Phases
Sound case			1.0589	1.0584	1.0583				0	Healthy
D_{th} = 1.1061 * 10^5										
LG	0.001	S1	14.104	1.1463	0.3998	12.958	0.7464	13.704	700.75	AG
LG	10	S2	10.856	0.5795	0.9739	10.277	0.3944	9.8822	376.49	AG
LG	100	S3	5.4440	1.1656	1.0555	4.2784	0.1101	4.3885	79.651	AG
LG	180	Teed point	3.7849	1.1517	1.0418	2.6332	1.0998	2.7431	33.715	AG
LG	400	S1	2.7330	1.0821	0.91422	1.6509	0.1690	1.8188	18.5244	AG
LG	600	S2	1.8739	1.1036	1.0659	0.77028	0.03772	0.8080	4.5295	Fail
LLG	0.001	S1	7.3280	7.3855	0	0.0574	7.3855	7.3280	738.61	ABG
LLG	10	S2	5.9170	7.1232	0.3894	1.2062	6.7338	5.5276	423	ABG
LLG	80	S3	5.0874	6.2306	1.1258	1.1431	5.1047	3.9616	207	ABG
LLG	120	Teed point	4.3478	5.0826	1.1309	0.7348	3.9517	3.2169	156.15	ABG
LLG	300	S2	2.599	2.7782	1.1492	0.17823	1.6289	1.4507	57.205	ABG
LLG	600	S3	1.8734	1.955	1.10	0.0890	0.8555	0.7734	30.44	ABG

The third correction factor is computed through the following equation:

$$\beta_3 = \frac{(r^2\beta_1 + 1)}{r^2} \tag{B.4}$$

The fourth correction factor is computed through the following equation:

$$\beta_4 = \frac{(\beta_2\beta_3 + \beta_2\beta_1 - 1)}{\beta_2} \tag{B.5}$$

Several studies have been carried out on different real system configuration different voltage levels as shown in Table B.1. It was found that the obtained correction factors are slightly changed. Further analysis has been done as mean value and average deviation functions for all factors to show the slight change between them. The proposed scheme is applied to different real network configurations at different voltage levels.

Also, it was tested at different fault conditions to clear how different correction factors can be implemented in real time applications.

For example, teed circuits 66 kV Delta realistic network [26] is used to verify of the proposed scheme on real application. The mean values of correction factors are used in proposed scheme and obtained results are summarized in Table B.2. It is cleared from simulation results in Table B.2 that the proposed scheme has ability to identify all ground fault types. However, it failed to identify single line to ground fault at high fault resistance upper than 550 Ω, the overall performance of proposed scheme is accepted. Consequently, when using the mean values of correction factors, the fault-identification ability of the proposed scheme has been found a good fault identification decision for given real applications.

References

[1] N. Zhang, M. Kezunovic, Transmission line boundary protection using wavelet transform and neural network, IEEE Trans. Power Del. 22 (2) (2007) 859–869.
[2] M. Da Silva, D. Coury, M. Oleskovicz, E.C. Segatto, Combined solution for fault location in three-terminal lines based on wavelet transform, IET Gener. Transm. Distrib. 4 (1) (2010) 94–110.
[3] S.M. Brahma, New fault-location method for a single multi-terminal transmission line using synchronized phasor measurements, IEEE Trans. Power Del. 21 (3) (2006) 1148–1153.
[4] R.P. Hasabe, A.P. Vaidya, Detection and classification of faults on 220 KV transmission line using wavelet transform and neural network, Int. J. Smart Grid Clean Energy 3 (3) (2014) 283–290.
[5] A.R. Adly, R.A. El Sehiemy, A.Y. Abdelaziz, A novel single end measuring system based fast identification scheme for transmission line faults, Measurement 103 (2017) 263–274.
[6] B. Bhalja, R.P. Maheshwari, Wavelet-based fault classification scheme for a transmission line using a support vector machine, Electr. Power Compon. Syst. 36 (2008) 1017–1030.
[7] A.R. Adly, R.A. El Sehiemy, A.Y. Abdelaziz, Critical aspects on wavelet transforms-based fault-identification procedures in HV transmission line, IET Gener. Transm. Distrib. 10 (2) (2016) 508–517.
[8] Z. Liu, Z. Han, Y. Zhang, Q. Zhang, Multi-wavelet packet entropy and its application in transmission line fault recognition and classification, IEEE Trans. Neural Networks Learn. Syst. 25 (11) (2014) 2043–2052.
[9] K. Thirumala, A.C. Umarikar, T. Jain, Estimation of single-phase and three-phase power-quality indices using empirical wavelet transform, IEEE Trans. Power Del. 30 (1) (2015) 445–454.
[10] Z. He, Z. Zhang, W. Chen, et al., Wide-area backup protection algorithm based on fault component voltage distribution, IEEE Trans. Power Del. 26 (4) (2011) 2752–2760.
[11] B. Mohamedi, Z.J. Gou, Fault classification and faulted phase selection based on the symmetrical component of reactive power for single –circuit transmission lines, IEEE Trans. Power Del. 28 (4) (2013) 2326–2332.
[12] Z.Y. He, X.P. Li, et al., Dynamic fault locator for three-terminal transmission lines for phasor measurement units, IET Gener. Transm. Distrib. 7 (2) (2013) 183–191.
[13] T. Wu, C.Y. Chung, I. Kamwa, et al., Synchrophasor measurement-based fault location technique for multi-terminal multi-section non-homogeneous transmission lines, IET Gener. Transm. Distrib. 10 (8) (2016) 1815–1824.
[14] Q. Jiang, B. Wang, X. Li, An efficient PMU-based fault-location technique for multi-terminal transmission lines, IEEE Trans. Power Del. 29 (4) (2014) 1675–1682.

[15] J. Izykowski et al., A fault-location method for application with current differential relays of three-terminal lines, IEEE Trans. Power Delivery 22 (4) (2007) 2099–2107.
[16] M.M. Eissa, A new digital relaying scheme for EHV three terminal transmission lines, Electr. Power Syst. Res. 73 (2005) 107–112.
[17] Z. Moravej, M. Movahhedneya, G. Radman, M. Pazoki, Effective fault location technique in three-terminal transmission line using hilbert and discrete wavelet transform, in: Electro/Information Technology (EIT), International Conference on IEEE, Dekalb, IL, USA, 2015, pp. 170–176.
[18] S.M. Brahma, Fault location scheme for a multi-terminal transmission line using synchronized voltage measurements, IEEE Trans. Power Del. 20 (2) (2005) 1325–1331.
[19] Y.H. Lin, C.W. Lin, C.S. Yu, A new fault locator for three-terminal transmission lines using two terminal synchronized voltage and current phasors, IEEE Trans. Power Del. 17 (2) (2002) 452–459.
[20] S. Hussain, A.H. Osman, Fault location scheme for multi-terminal transmission lines using unsynchronized measurements, Int. J. Electr. Power Energy Syst. 78 (2016) 277–284.
[21] B. Mahamedi, M.S. Pasand, S. Azizi, J.G. Zhu, Unsynchronized fault-location technique for three-terminal lines, IET Gener. Transm. Distrib. 9 (15) (2015) 2099–2107.
[22] H. Livani, C.Y. Evrenosoğlu, A fault classification and localization method for three-terminal circuits using machine learning, IEEE Trans. Power Del. 28 (4) (2013) 2282–2290.
[23] A.Y. Abdelaziz, M. Abdel Rahman, M.S. Moussa, Distance protection for multi-terminal transmission lines, Electric Power and Energy Conversion Systems (EPECS), 2011 2nd International Conference on, IEEE, 2011.
[24] K. Saravanababu, P. Balakrishnan, K. Sathiyasekar, Transmission line faults detection, classification, and location using discrete wavelet transform, in: International Conference on Power, Energy and Control, Sri Rangalatchum Dindigul, India, 2013, pp. 233–238.
[25] Y. Tian, F. Chunju, Z. Gong, Pattern recognition-based fault classification for the teed transmission line, in: 2017 3rd International Conference on Advances in Electrical, Electronics, Information, Communication and Bio-Informatics (AEEICB) on IEEE, Chennai, India, 2017, pp. 441–445.
[26] Y.M. Sree, G.R. Kumar, M. Vaidehi, G. Priya, Wavelet approach for transient current based multi-terminal transmission system protection scheme in the presence of SVC, in: International Conference on Electrical, Electronics, and Optimization Techniques (ICEEOT) on IEEE, Chennai, India, 2016, pp. 4134–4140.
[27] F. Peng, J. Lai, Generalized instantaneous reactive power theory for three-phase power systems, IEEE T Instrum. Meas. 45 (1996) 293–297.
[28] G. Gökmen, Wavelet based instantaneous reactive power calculation method and a power system application sample, Int. Rev. Mod. Sim. 4 (2011) 745–752.
[29] X. Lin, Y. Gao, P. Liu, A novel scheme to identify symmetrical faults occurring during power swings, IEEE Trans Power Del. 23 (1) (2008).
[30] S. Jamali, A. Kazemi, H. Shateri, Comparing series and shunt reactive power compensation via UPFC from distance relay point of view, in: IEEE PES Transmission and Distribution Conf., New Orleans, LA, USA, April 19–22, 2010, pp. 1–6.
[31] Matthew Weiss, A. Chakrabortty, et al., A wide-area SVC controller design using a dynamic equivalent model of WECC, in: Power & Energy Society General Meeting, 2015 IEEE, IEEE, 2015, pp. 1–5.
[32] G. Chavan, M. Weiss, A. Chakrabortty, et al., Identification and predictive analysis of a multi-area WECC power system model using synchrophasors, IEEE Trans. Smart Grid 8 (4) (2017) 1977–1986.
[33] X. Jiang, J.H. Chow, Transfer path stability enhancement by voltage-sourced converter-based FACTS controllers, IEEE Trans. Power Del. 25 (2) (2010) 1019–1025.
[34] Ragab El Sehiemy, Walaa Sakr, A. Azmy, Optimal allocation of TCSCs by adaptive DE algorithm, IET Gener. Transm. Distrib. 10 (15) (2016) 3844–3854.
[35] Ahmed R. Adly, Ragab A. El-Sehiemy, Almoataz Y. Abdelaziz, Said A. Kotb, An accurate technique for discrimination between transient and permanent faults in transmission networks, Electr. Power Compon. Syst. 45 (4) (2017) 366–381.
[36] M.I. Zaki, R.A. El Sehiemy, G.M. Amer, et al., Integrated discrete wavelet transform-based faulted phase identification for multi-terminals power systems, in: IEEE Nineteenth International Middle East Power Systems Conference (MEPCON), 2017, pp. 503–509.
[37] A.G. Shaik, R.V. Pulipaka, A new wavelet-based fault detection, classification and location in transmission lines, Electric. Power Energy Syst. 64 (2015) 35–40.
[38] L.N. Tripathy, M.K. Jena, S.R. Samantaray, Differential relaying scheme for a tapped transmission line connecting UPFC and wind farm, Electric. Power Energy Syst 60 (2014) 245–257.
[39] H. Saadat, Power System Analysis, second ed., Mc Graw-Hill, NewYork, 2002.
[40] C. Bayliss, B. Hardy, Tansmission and Distribution Electrical Engineering, fourth ed., Elsevier, 2011.
[41] C. Kim, H. Kim, Y. Ko, S. Byun, A novel fault-detection technique of high-impedance arcing faults in transmission lines using the wavelet transform, IEEE Trans. Power Del. 17 (4) (2002) 921–929.
[42] F.B. Costa, Fault-induced transient detection based on real-time analysis of the wavelet coefficient energy, IEEE Trans. Power Del. 29 (1) (2014) 140–153.
[43] W.C. Santos, F.V. Lopes, N.S.D. Brito, et al., High impedance fault-identification on distribution networks, IEEE Trans. Power Del 26 (4) (2016) 1–8.
[44] J. Ren, M. Kezunovic, Elimination of DC offset in accurate phasor estimation using recursive wavelet transform, 2009 IEEE Bucharest Power Tech Conference, June 28th-July 2nd, Bucharest Romania, 2009.
[45] K. Chen, Caowei Huang, Jinliang He, Fault detection, classification and location for transmission lines and distribution systems: a review on the methods, High Volt. 1 (1) (2016) 25–33.